J Mater Sci (2010) 45:2510–2517
DOI 10.1007/s10853-010-4223-z

Effects of yttrium and zinc addition on the microstructure and mechanical properties of Mg–Y–Zn alloys

Bin Chen · Dongliang Lin · Xiaoqin Zeng · Chen Lu

Received: 19 March 2009 / Accepted: 11 January 2010 / Published online: 5 February 2010

Abstract The effects of the yttrium and zinc additions on microstructure and mechanical properties of Mg–Y–Zn alloys were investigated. It was found that the addition of yttrium increases the eutectic temperature of Mg–Y–Zn alloys greatly. The addition of yttrium can also greatly increase the dynamic recrystallization (DRX) temperature of Mg–Y–Zn alloys. The volume fraction of DRX grains in $Mg_{97}Y_2Zn_1$ alloy is larger than that in $Mg_{96}Y_3Zn_1$ alloy but smaller than that in $Mg_{95.5}Y_3Zn_{1.5}$ alloy due to the effects of yttrium and zinc addition. The long period stacking (LPS) structures of 18R and 14H were observed in Mg–Y–Zn alloys. The increase in the yttrium content results in increase in strength and decrease in elongation in Mg–Y–Zn alloys. The increase in both yttrium and zinc contents results in increase in both strength and elongation in Mg–Y–Zn alloys. The high strengths of the alloys were thought due to the strengthening by the grain refinement, solid solution strengthening, strain strengthening, high density of plane faults of the LPS structures, and distribution of fine $Mg_{24}Y_5$ phase.

Introduction

Recently, it was found that $Mg_{97}Y_2Zn_1$ (at.%) processed by rapid solidified powder metallurgy (RS/PM) reveals excellent mechanical properties with high yield strength (YS) of 610 MPa and elongation of 5%, respectively, at room temperature. Its high strength was thought due to the strengthening by the grain refinement, solid solution, fine $Mg_{24}Y_5$ compound particles, and an introduction of a high density of plane faults caused by the formation of the long period stacking (LPS) structure [1]. In other researches, the LPS structure was also found in the $Mg_{97}Y_2Zn_1$ alloys prepared by rapidly solidified ribbon [2] and Cu-mold casting [3]. Rapidly solidification followed by equal channel angular pressing was also attempted [4]. The $Mg_{97}Y_2Zn_1$ alloys produced by ingot metallurgy, chipped powder metallurgy, and RS/PM processing were also reported [5]. However, the effects of alloying additives of yttrium and zinc on the Mg–Y–Zn alloys in equilibrium state remain unknown. This article focused on the ingot metallurgy and extrusion of Mg–Y–Zn alloys with different yttrium and zinc additions. The effects of the yttrium and zinc additions on microstructure and mechanical properties of Mg–Y–Zn alloys were investigated.

B. Chen · D. Lin (✉) · X. Zeng · C. Lu
School of Materials Science and Engineering, Shanghai Jiao Tong University, Shanghai 200240, People's Republic of China
e-mail: dllin@sjtu.edu.cn

B. Chen
e-mail: steelboy@163.com

Experimental procedure

The alloys $Mg_{98}Y_1Zn_1$ (alloy 1), $Mg_{97}Y_2Zn_1$ (alloy 2), $Mg_{96}Y_3Zn_1$ (alloy 3), $Mg_{95.5}Y_3Zn_{1.5}$ (alloy 4), and $Mg_{94}Y_4Zn_2$ (alloy 5) were fabricated by adding pure zinc and Mg–25%Y master alloy to pure magnesium melt at about 1023 K using a mild steel crucible in an electric resistance furnace under a protecting gas (0.3%SF_6 and 99.7%CO_2). The melt was held for 30 min and then poured into a mild steel mold that was preheated to 473 K. The ingots were homogenized at 833 K for 12 h and then air cooling. The ingot of alloy 1 was heat treated at 813 K for 15 h and the ingots of alloys 2–5 were heat treated at 833 K for 12 h. The alloy 1 was hot extruded into rods with the extrusion ratio 26.9:1 at 603 K. The alloys 2–4 were

extruded successfully until extrusion ratio decreased to 12.25:1 and temperature increased to 673 K. Alloy 5 even cannot be extruded at these conditions.

The tensile tests were conducted on Zwick electronic universal material testing machine at room temperature. The solution and eutectic temperatures of second phases in the alloys were studied via differential thermal analysis (DTA) at a heating rate of 10 K/min. The compositions of alloys were determined by an inductively coupled plasma-atomic emission spectrometry. The phase analyses were carried out with a D/max 2550 V X-ray diffractometer (XRD). The energy dispersion spectroscopy (EDS) was performed in the EDAX-equipped scanning electron microscopy (SEM). The microstructure was characterized by an optical microscope and a SEM. The samples were etched with acetic picral (10 mL acetic acid, 4.2 g picric acid, 10 mL H_2O, 70 mL ethanol). Transmission electron microscopy (TEM) observation was performed using JEOL-2010 operating at 200 kV. The TEM samples were thinned at 233 K with a twin-jet polisher under the conditions of 20 mA and 75 V by using a solution of 5% $HClO_4$ in ethanol. Further thinning to a thickness of electron transparency was carried out by using ion milling.

Results and discussion

Microstructure of as-cast Mg–Y–Zn alloys

Figure 1 shows the optical micrographs of as-cast alloys 1–5, respectively. It shows that the secondary phase distributed along grain boundaries. The lamellar structure can be observed in the secondary phase. With the yttrium content increasing (Fig. 1a–c) or yttrium and zinc total

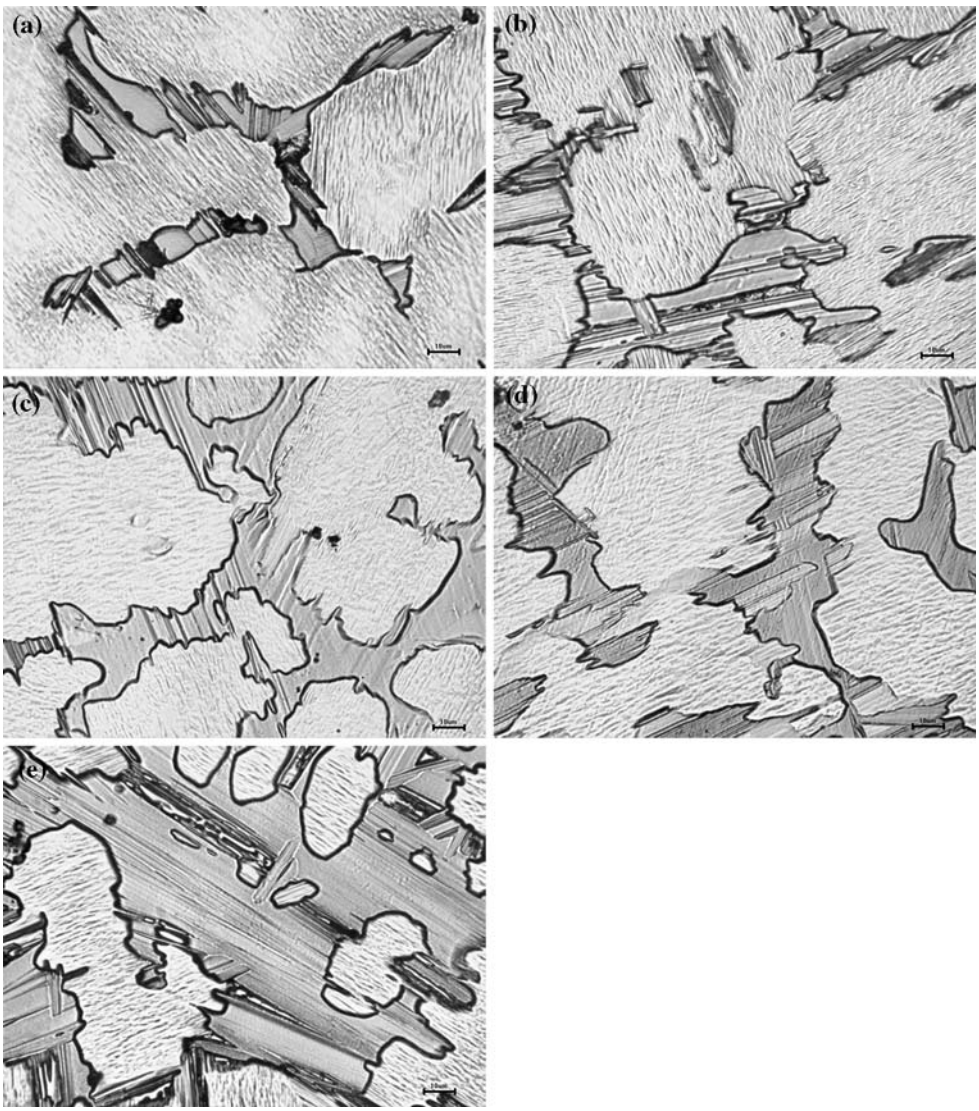

Fig. 1 Optical micrographs of as-cast Mg–Y–Zn alloys: **a** alloy 1, **b** alloy 2, **c** alloy 3, **d** alloy 4, **e** alloy 5

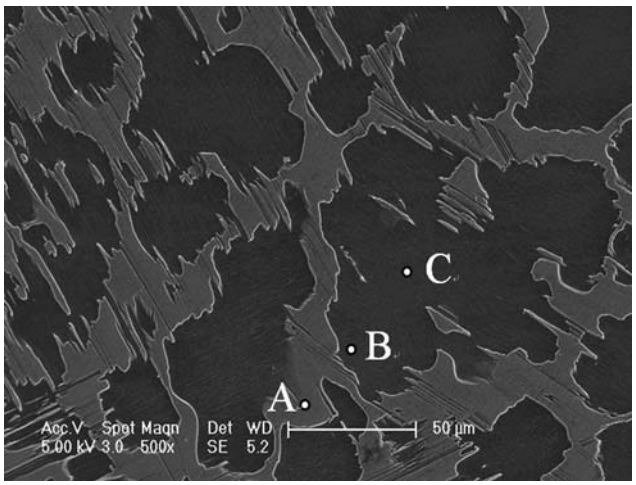

Fig. 2 The SEM microstructure images of the as-cast $Mg_{97}Y_2Zn_1$ alloy

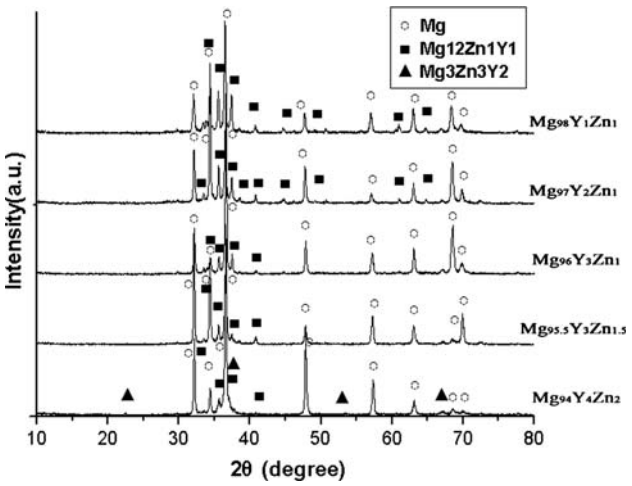

Fig. 3 XRD pattern of the as-cast Mg–Y–Zn alloys

contents increasing (Fig. 1b, d, and e), the secondary phases change from discontinuous network distribution into continuous network distribution. The widths of the secondary phases are also increased progressively.

The element contents of alloys were analyzed by EDS. For example, three areas A (the secondary phase), B (matrix near the secondary phase), and C (the center of matrix) were chosen in $Mg_{97}Y_2Zn_1$ alloy, as shown in Fig. 2. The EDS results show the composition of areas A, B, and C are Mg–7.13 at.%Y–6.25 at.%Zn, Mg–2.00 at.%Y–1.03 at.%Zn, and Mg–0.70 at.%Y–0.86 at.%Zn, respectively. It is obviously that the Y and Zn contents in matrix relate to its distance to the secondary phase.

The fine lamellar structure can be observed inside matrix. In Fig. 1b–e, the entire matrix is covered with the fine lamellar structure. But in alloy 1, the fine lamellar structure only appears by the secondary phase, as shown in Fig. 1a. It also indicates that there is a correlation between the formation of fine lamellar structure and the segregation of yttrium and zinc. In alloys 2–5, the fine lamellar structure occurs at the whole matrix due to it contains high composition of yttrium and zinc. In alloy 1, however, the fine lamellar structure only formed in the matrix near the secondary phase where contain high composition of yttrium and zinc. It illuminates that the fine lamellar structure originates from solid solution of saturated with yttrium and zinc, and its distribution related to segregation of yttrium and zinc.

Figure 3 shows the XRD pattern of as-cast alloys 1–5. The pattern indicates that the alloy 1 is consists of α-Mg, W-$Mg_3Zn_3Y_2$ (cubic structure) [6], and X-$Mg_{12}ZnY$ (a long-period 18R modulated structure) [7]. However, there is no $Mg_3Zn_3Y_2$ in alloys 2–5. It indicates that the $Mg_{12}ZnY$ exist in Mg–Y–Zn alloys with relative high Y/Zn ratio [8]. It also illuminates that alloy 2 promote the

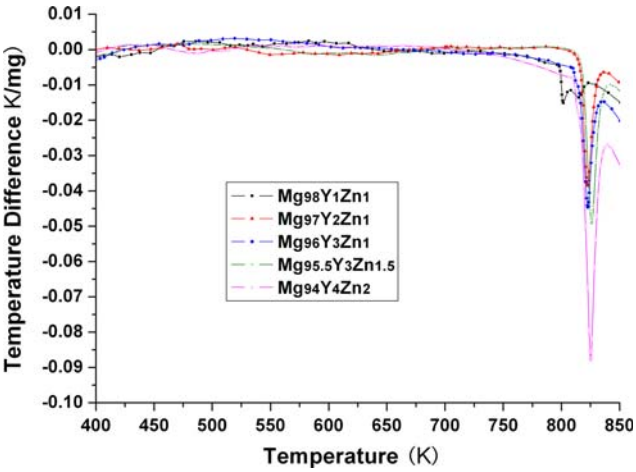

Fig. 4 DTA traces of the as-cast Mg–Y–Zn alloys

formation of X-phase, although alloy 1 has same proportion of yttrium and zinc with X-phase.

Figure 4 shows the DTA results of the as-cast alloys during the heating process. For alloys 2–5, the first endothermic peak appeared at about 823 K. Because these alloys contain only one secondary phase, i.e., X-phase, this peak corresponds to the melting temperature of X-phase eutectic pocket [9]. On these DTA curves, there is another endothermic peak at about 903 K. These peaks are related to the melting temperature of α-Mg. For alloy 1, the first endothermic peak appeared at about 803 K. Because alloy 1 contains W-phase, this peak corresponds to the melting temperature of W-phase eutectic pocket. From the DTA study, the lowest eutectic temperature of alloy is about 803 K, which is much higher than the eutectic temperature of Mg–Zn binary alloys (613 K) [10]. It can be inferred that the addition of yttrium can greatly increase the eutectic temperature of Mg–Y–Zn alloys [11].

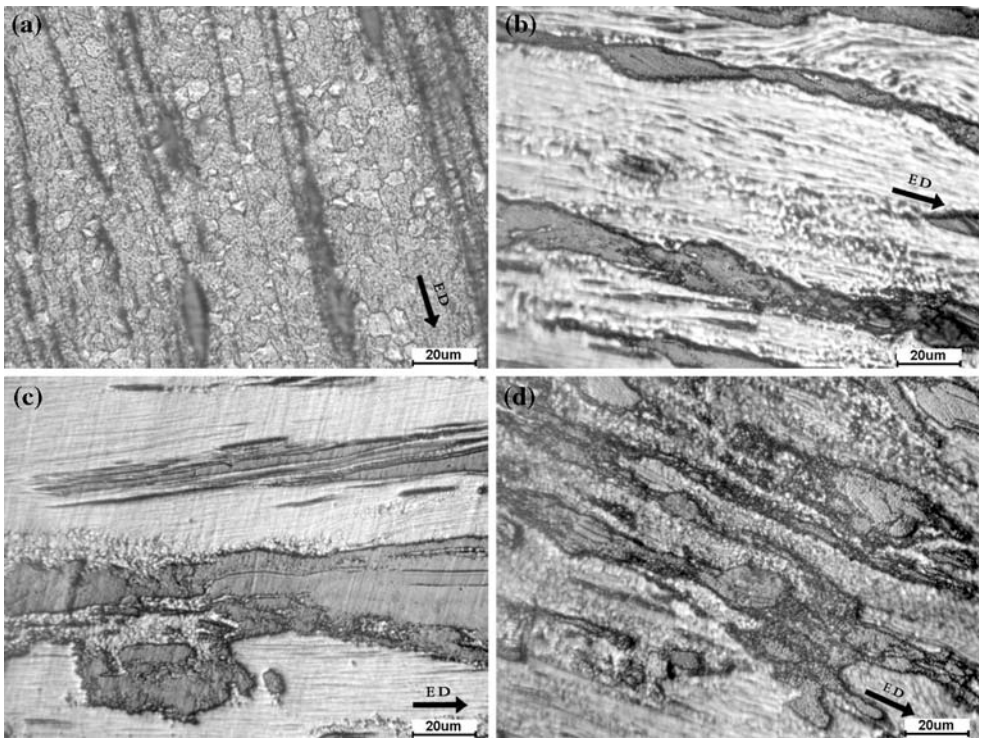

Fig. 5 Optical micrographs of extruded Mg–Y–Zn alloy: **a** alloy 1, **b** alloy 2, **c** alloy 3, and **d** alloy 4

Microstructure of extruded Mg–Y–Zn alloys

Figure 5 shows the optical micrographs of typical extruded alloys 1–4. In these images, the original network distributed secondary phases had been deformed into stringers of secondary phase particles along the extrusion direction. With the yttrium and zinc content increasing, the denser secondary phases were seen. Figure 5a shows that the alloy 1 was dominated by equiaxed dynamic recrystallization (DRX) grains after extrusion. It illuminates that the DRX had completed in alloy 1. However, the DRX process was incomplete, as shown in Fig. 5b–d. The streamline can be observed in the matrix.

The observation of DRX in extruded alloys 2–4 were performed by SEM, as shown in Fig. 6. Figure 6a shows that many fine DRX grains formed around secondary phase particles and distorted grains boundaries in extruded alloy 2. This suggests that accumulated dislocations at particles and grain boundaries stimulated the DRX process [12]. However, the DRX process was incomplete. This can be ascribed that the yttrium addition increases the DRX temperature of the alloy. In the same way, the DRX process had hardly occurred in alloy 3 due to higher yttrium addition, as shown in Fig. 6b. However, the DRX processes advanced much in alloy 4, as shown in Fig. 6c, although it was still incomplete. The volume fraction of DRX grains in alloy 4 is much larger than that in either alloy 2 or 3. Obviously, it is due to the higher zinc addition decreased the DRX temperature. The element contents of areas A, B, C, D, and E, as marked in Fig. 6 are analyzed by EDS. The element contents are given in Table 1. The EDS results show the composition of Zn in areas A, B, and E is close to each other. However, the average content of Y in areas B and E is higher than that in area A due to higher Y addition. It is obviously that the average content of Y and Zn in area C of secondary phase is higher than that in matrix. These secondary phases can be defined as X-phase. There are some fine bright phases in each alloy, such as phases in the area D. The EDS analysis shows that the average content of Y and Zn in the area D is the highest in alloy. It illustrates that these fine bright phases are $Mg_{24}Y_5$ phases.

TEM observation of Mg–Y–Zn alloys

The TEM micrographs and its selected area diffraction patterns (SADPs) of as-cast alloy 2 are shown in Fig. 7. As can be seen from Fig. 7a, the secondary phase shows wide lamellar structure. There are some fine lamellar structures that can be observed in the area of α-Mg, as marked by arrow. The fine lamellar structures are parallel to the neighboring secondary phases. The SADPs of the area marked by A, B, and C were also inserted in Fig. 7. As can be seen from Fig. 7b, the structure of the area A is clearly recognized as 2H–Mg. In Fig. 7c, however, the extra reflection-spots are evident at positions of $n/9$ (0002) hcp (n is an integer) in c^*-direction. It is obvious that secondary phase presents 18R LPS structure. Figure 7d demonstrated

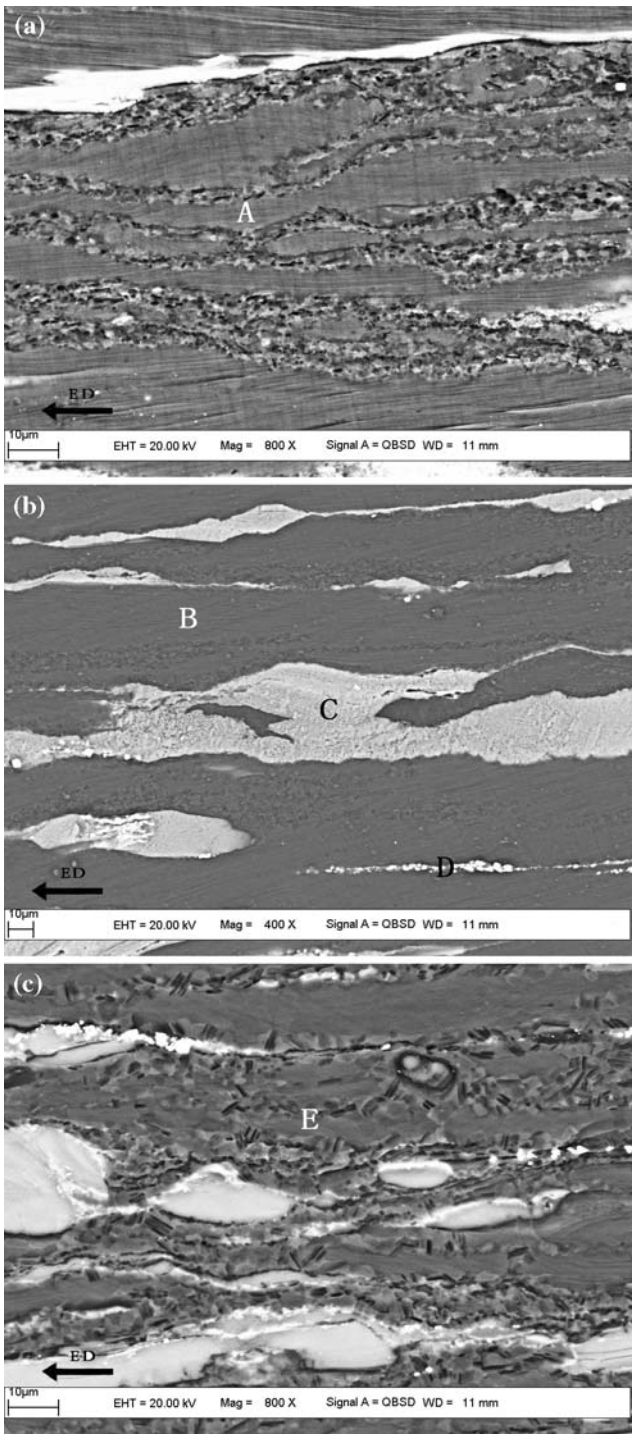

Fig. 6 SEM micrographs of extruded Mg–Y–Zn alloy: **a** alloy 2, **b** alloy 3, and **c** alloy 4

that the phase in square shape is $Mg_{24}Y_5$. The fine $Mg_{24}Y_5$ is also observed in the alloys series despite it has not been detected by XRD pattern. As shown in Fig. 7e, f, both chemical compositions of α-Mg and secondary phase contain Mg, Y, and Zn by EDS spectra. Contents of yttrium and zinc in α-Mg are significantly less than that in the secondary phase. The compositions in α-Mg and secondary phase are Mg–0.88 at.%Y–0.05 at.%Zn and Mg–7.42 at.%Y–5.43 at.%Zn, respectively. It also confirms that the formation of fine LPS structure in matrix was attributed to the dissolution of a certain amount of yttrium and zinc in α-Mg.

Table 1 Chemical composition distribution of as-extruded Mg–Y–Zn alloys

Element	Area				
	A	B	C	D	E
Mg	97.20	96.52	86.26	62.42	96.36
Zn	0.87	0.81	5.77	13.84	0.87
Y	1.93	2.67	7.98	23.74	2.77
Totals	100.00	100.00	100.00	100.00	100.00

The TEM micrograph and SADP of alloy 2 after extrusion are shown in Fig. 8. Figure 8a shows that there is a fine lamellar structure inside grain. The SADP shows the extra reflection-spots at c^*-direction, as shown in Fig. 8b, c. Although the extra reflection-spots are weak, we still can identify it as 14H structure [13].

Mechanical properties of extruded Mg–Y–Zn alloys

The mechanical properties of extruded alloy 1 are quite different from alloys 2–4. The extruded alloy 1 has excellent ductility with the elongation of 24%. Its strengths are comparatively low with YS of 192 MPa and ultimate tensile strength (UTS) of 282 MPa, respectively. Compare with alloy 1, alloys 2–4 have high strength but low elongation. Figure 9 represents the comparisons of the mechanical properties of extruded alloys 2–4 at both ambient temperature and elevated temperature. The UTS of the extruded alloys is increased significantly to 400 MPa at ambient temperature which is considerable high strength for magnesium alloy. The high strength of alloys is due to that the LPS structures suppress the cross-slip and the climb of dislocations, as well as the basal slip [14]. With the temperature increase, the strength decreases and the elongation increases progressively. Especially, there is an abrupt fall of strengths at 523 K. The necking phenomenon of tensile specimens also appears at 523 K, as shown in Fig. 10. It due to that the deformation is controlled by extensively non-basal slip at the temperature [15]. Even so, alloys 2–4 still have UTS of about 290 MPa at 523 K. The outstanding mechanical properties at elevated temperature are attributed to high thermal stability of the LPS structure and $Mg_{24}Y_5$ (melting temperature of 840 K [16]). As a result, elevated temperature behavior of alloys 2–4 suppose that the alloys can be used at the condition of relative high temperature.

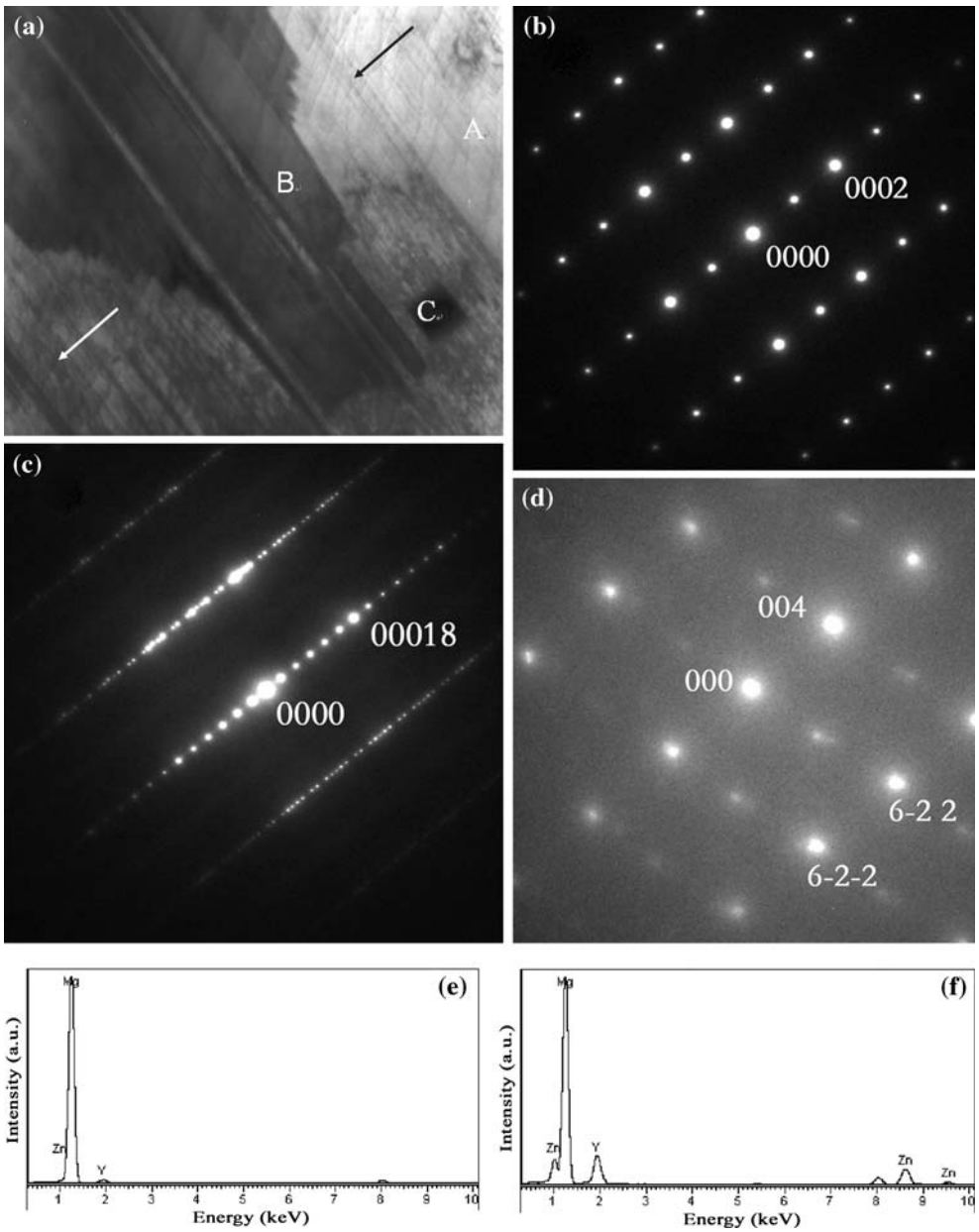

Fig. 7 **a** TEM micrograph of as-cast alloy 2. Electron diffraction pattern taken from **b** area A, **c** area B, and **d** area C marked in (**a**). Typical EDS spectra obtained from **e** area A and **f** area B

The contrast of mechanical properties between alloy 1 and other three alloys were investigated firstly. Low yttrium-added alloy such as alloy 1 has low strength but high elongation. With proportion between yttrium and zinc increased to 2:1 or more, the Mg–Y–Zn alloys exhibit high strength and low elongation comparatively. It is due to that yttrium and zinc in the proportion of 2:1 promote the formation of LPS structure, as mentioned above. The distribution of LPS structure as well as fine $Mg_{24}Y_5$ phase in matrix increases strength. On the other hand, the secondary phase with LPS structure distributed heterogeneously at the grain boundary decrease the elongation. From Fig. 11, the cracks preferentially initiated and propagated at interior of the X-phase instead of at the interface of X-phase/α-Mg during tensile deformation due to that the X-phase has the axis-to-axis orientation relationship with magnesium matrix [7]. The $Mg_{97}Y_2Zn_1$ alloy contain high volume fraction of X-phase and resulted in premature fracture and lower elongation.

By comparison of alloys 2 and 3, it was found that merely increase in the yttrium content results in increase in strength and decrease in elongation both at room temperature and elevated temperature. The strength improvement of alloy 3 is probably attributed to the more distribution of

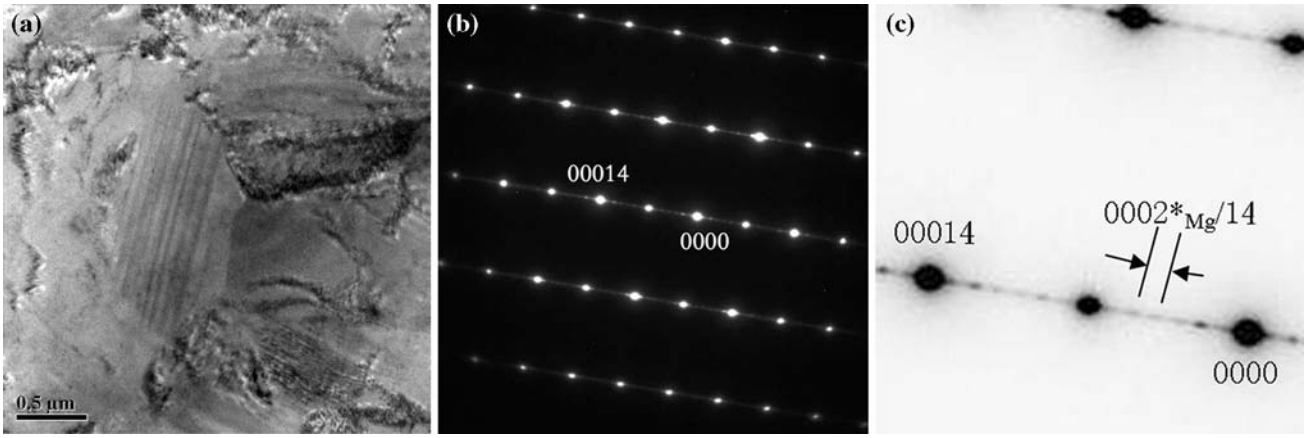

Fig. 8 **a** TEM micrograph and **b** SADP of the extruded alloy 2, **c** enlargement of **b**

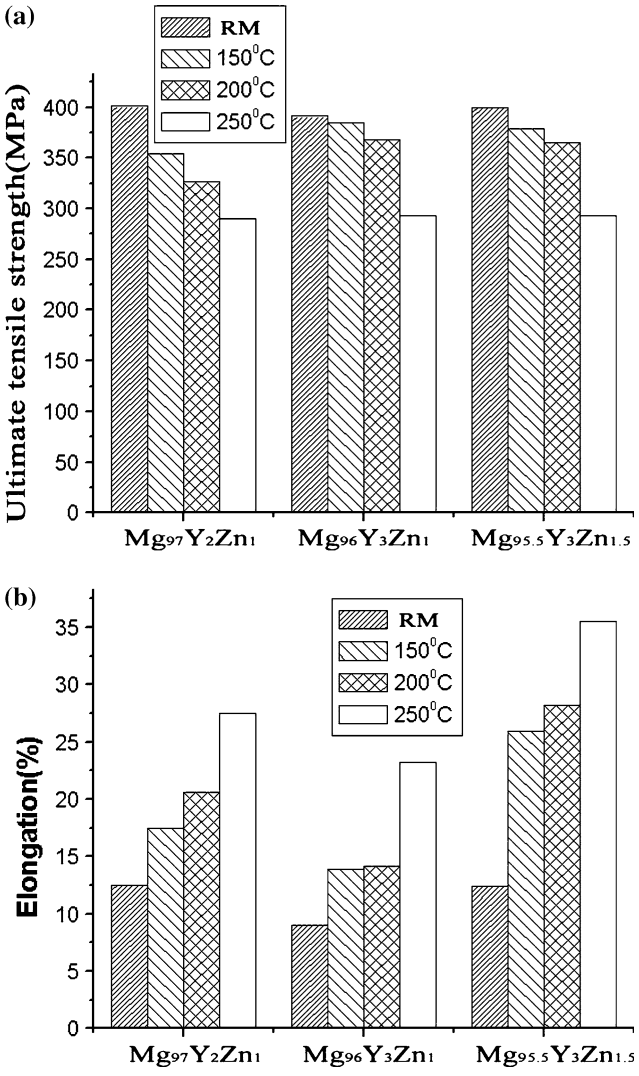

Fig. 9 **a** The UTS and **b** elongation of the extruded Mg–Y–Zn alloys at both ambient temperature and elevated temperature

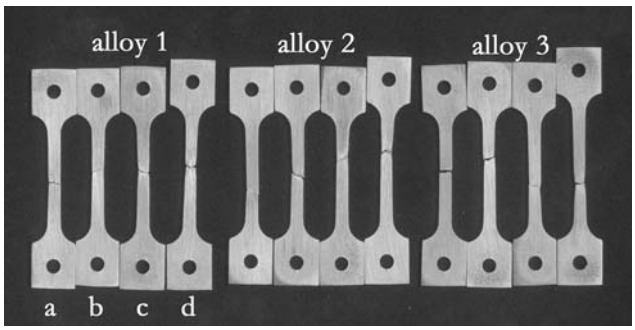

Fig. 10 Tensile specimens after deformation at *a* room temperature, *b* 423 K, *c* 473 K, and *d* 523 K

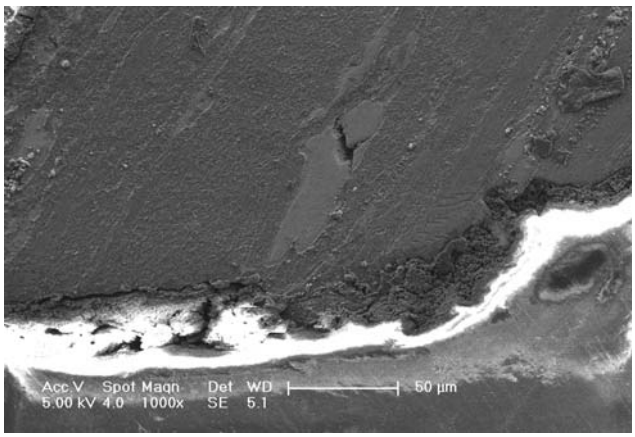

Fig. 11 The SEM morphology for the vertical section of the test specimen of extruded $Mg_{96}Y_3Zn_1$ alloy ruptured by tensile test

fine $Mg_{24}Y_5$ phase [17]. The extra addition of yttrium is consumed by formation of $Mg_{24}Y_5$ phase instead of formation of LPS structure. Fine $Mg_{24}Y_5$ contributes significantly to the hindrance of grain boundary slip and matrix

deformation but promotes brittleness [18]. Alloy 3 also presents the highest strength in three alloys at elevated temperature.

Comparison alloy 2 with alloy 4, it is obvious that increasing both yttrium and zinc contents can improve the mechanical properties remarkably. From Fig. 9, alloy 4 has similar mechanical properties with alloy 2 at room temperature. But its mechanical properties at elevated temperature are much better than alloy 2. Its improved mechanical properties at elevated temperature are attributed to the more formation of LPS structure. It also presents the highest elongation in these three alloys.

As mentioned above, we can get a conclusion that yttrium and zinc addition plays very important role in mechanical properties of extruded Mg–Y–Zn alloys. The excellent mechanical properties of the alloys were thought due to the strengthening by the grain refinement, solid solution strengthening, strain strengthening, high density of plane faults of the LPS structures, and distribution of fine $Mg_{24}Y_5$ phase.

Conclusions

In this article, Mg–Y–Zn alloys prepared by casting and extrusion have been investigated. It was found that the yttrium and zinc addition plays very important role on microstructure and mechanical properties of Mg–Y–Zn alloys. The obtained results are summarized as follows.

(1) The addition of yttrium increases the eutectic temperature of Mg–Y–Zn alloys greatly.
(2) The addition of yttrium can greatly increase the DRX temperature of Mg–Y–Zn alloys. The addition of zinc can decrease the DRX temperature of Mg–Y–Zn alloys. The volume fraction of DRX grains in alloy 2 is larger than that in alloy 3 but smaller than that in alloy 4 due to the effects of yttrium and zinc addition.
(3) The LPS structures of 18R and 14H were observed in Mg–Y–Zn alloys.
(4) The increase in the yttrium content results in increase in strength and decrease in elongation in Mg–Y–Zn alloys.
(5) The increase in both yttrium and zinc contents results in increase in both strength and elongation in Mg–Y–Zn alloys.
(6) The high strengths of the alloys were thought due to the strengthening by the grain refinement, solid solution strengthening, strain strengthening, high density of plane faults of the LPS structures, and distribution of fine $Mg_{24}Y_5$ phase.

Acknowledgement This research was supported by the National Natural Science Foundation of China (Grant No. 50471015).

References

1. Inoue A, Kawamura Y, Matsushita M, Hayashi K, Koike J (2001) J Mater Res Soc 16:1894
2. Nishida M, Yamamuro T, Nagano M, Morizono Y, Kawamura Y (2003) Mater Sci Forum 419–422:715
3. Itoi T, Seimiya T, Kawamura Y, Hirohashi M (2004) Scr Mater 51:107
4. Yoshikawa M, Kohzu M, Watanabe H, Higashi K (2003) Mater Sci Forum 419–422:769
5. Kawamura Y (2005) Proceedings of the 1st Asian symposium on magnesium alloys. p 25
6. Lee JY, Kim DH, Lim HK, Kim DH (2005) Mater Lett 59:3801
7. Luo ZP, Zhang SQ (2000) J Mater Sci Lett 191:813
8. Shao G, Varsani V, Fan Z (2006) Calphad 30:286
9. Feng JN, Guo XF, Xu CJ, Zhang ZM (2006) J Chin Rare Earth Soc 24:86
10. Bhan S, Lal A (1993) J Phase Equilib 14:634
11. Padezhnova EM, Melnik EV, Miliyevskiy RA, Dobatkina TV, Kinzhibalo VV (1982) Russ Metall (Metally) 4:185 (English translation)
12. Humphreys FJ, Hatherly M (1995) Recrystallization and related annealing phenomena. Pergamon Press, Oxford
13. Matsuda M, Ii S, Kawamura Y, Ikuhara Y, Nishida M (2005) Mater Sci Eng A 393:269
14. Suzuki MI, Kimura T, Koike J, Maruyamaa K (2004) Mater Sci Eng A 387–389:706
15. Garcés G, Maesoa M, Todd I, Pérez P, Adeva P (2007) J Alloys Compd 432:L10
16. Okamoto H (2006) J Phase Equilib Diff 27:431
17. Chen B, Lu C, Lin D, Zeng X (accepted) Mater Sci Forum
18. Liang WZ, Ning ZL, Wang HB, Liu HD, Liu HH (2004) J Rare Earth 22:268